Bioinformatic and Experimental Analysis Reveals Knockdown of KIF15 Promotes Cell Apoptosis via Activating Crosstalk of Multi-Pathways in Ovarian Cancer

Xinwei Sun
Army Medical University
Mengyue Chen
First People's Hospital of Chongqing Liang Jiang New Area: The First People's Hospital of Chongqing Liangjiang New Area
Bin Liao
University of the Chinese Academy of Sciences
Zhiqing Liang (zhiqingliang2020@163.com)
Army Medical University https://orcid.org/0000-0002-8608-2857

Research

Keywords: Ovarian Neoplasms, Kinesin, Prognosis, Early diagnosis, Molecular targeted therapy, Cell proliferation, Apoptosis

Posted Date: September 8th, 2020

DOI: https://doi.org/10.21203/rs.3.rs-72091/v1

Abstract

Background: Ovarian cancer (OC) is the most lethal malignancy of females worldwide. Unlimited proliferation is a fundamental feature of OC cells. The genes associated with cell proliferation are potential histopathological biomarkers and targets of anti-tumor therapeutic strategies. In the present study, we aimed to identify proliferation-associated biomarkers with potential prognostic, diagnostic, and therapeutic value and reveal the underlying molecular mechanism of the candidate gene involved in OC by a combination of bioinformatic and experimental methods.

Results: KIF15 was upregulated in early-stage OC tissues and could predict poor prognosis of patients of Stage I and II. The knockdown of KIF15 significantly inhibited cell proliferation, tumor formation, and growth as well as promoted apoptosis of OC cells. A combination of experimental and bioinformatic analyses revealed KIF15 knockdown promoted cell apoptosis via activating crosstalk of multi-pathways in OC.

Conclusion: In this study, KIF15, an early-stage prognostic gene, was identified as a potential histopathological biomarker and therapeutic target of OC.

Background

OC ranks as the first lethal tumor that occurs in female reproductive organs. The incidence of this gynecological malignancy has been continuously increasing each year. In 2018, there were approximately 22,240 newly diagnosed OC cases and 14,070 deaths of OC in the United States [1]. The poor prognosis of OC mainly due to the lack of reliable diagnostic and prognostic biomarkers especially in early stages. The two serum biomarker of OC, Cancer Antigen 125 (CA125) and Human Epididymis Protein 4 (HE4), was used to detect the fatal disease globally. Although the specificity of CA125 + HE4 reached to 82.85% and the sensitivity reached to 92.18%, the combined measure did the little too early diagnosis and prognosis of OC [2]. Thus, despite the surgical techniques have been improved and new chemotherapeutic agents such as PARP inhibitors [3] have been applied to clinical treatment, the improvement of OS in OC patients are still unsatisfactory. There is a desperate need for biomarkers of early prognostic indicators, as well as novel histopathological diagnostic biomarkers and therapeutic targets.

With the genomic technologies rapidly developing in recent years, large amounts of high-throughput data have been generated. The genome-wide RNA expression analysis has become a frequently used tool for researchers to screen and understand the genes which play key roles in tumorigenesis and progression. A variety of high-throughput platforms such as GEO [4] and the Cancer Genome Atlas (TCGA) [5] can be available to identify genes that might serve as early prognostic and histopathological diagnostic biomarkers or even contribute to targeted therapies. Otherwise, integrated analysis by multiple bioinfomatics methods can also provide crucial clues for a better understanding of the molecular mechanism that the candidate genes were involved in a certain kind of tumor.

Researchers have been focusing on identifying prognostic and diagnostic biomarkers as well as therapeutic targets of OC by bioinformatic methods. In a study, 226 overlapped DEGs were identified by using the mRNA expression profile of GSE14407, GSE18520, GSE26712, and GSE54388. The gene ontology (GO) analysis showed that genes were significantly enriched in the biological process of the G2/M transition of the mitotic cell cycle, the apoptotic process, and cell proliferation [6]. In another study, 190 consistent DEGs were identified by analyzing the data of GDS3592, GSE54388, and GSE66957. The GO categories included cell proliferation, adhesion, and differentiation and intracellular signal cascades [7]. Previous studies have shown that many DEGs were enriched to the biological process (BP) of cell proliferation in OC. Unlimited proliferation is a fundamental characteristic of cancer cells. Being an important part of tumor growth and progression, proliferation has been studied as a target of anti-tumor therapeutic interventions for years [8]. We expect that we can obtain potential therapeutic targets with an early prognostic and histopathological diagnostic value from the proliferation signatures to better understand the cancer pathogenesis and to improve the survival of OC. To identify more reliable biomarkers, integrated bioinformatic analyses combined with experimental verification would be performed.

In the present research, we identified 40 proliferation-associated genes from 190 consistent DEGs between ovarian cancer and non-tumor specimens by analyzing the gene expression profiling of four GEO datasets. The Kalplan-miere Plotter [9] was used to identify survival-related candidate genes. Thus, we obtained only two genes (KIF15 and BUB1 Mitotic Checkpoint Serine/Threonine Kinase B [BUB1B]) which overexpressed and had a significant effect on OS in early-stage OC patients. Otherwise, we found KIF15 had a higher expression level in early stages than that of late stages, suggesting a possibility to be an early-stage histopathological biomarker of prognosis and diagnosis. Therefore, KIF15 was selected to be bioinformatically and functionally analyzed subsequently. Our study certificated that KIF15 was a proliferation-associated gene with a potential value of early prognosis and diagnosis in OC. Knockdown of KIF15 activated OC cell apoptosis through crosstalk among multi pathways, indicating the possibility for KIF15 to be a therapeutic target of OC. These findings can provide reliable shreds of evidence for early prognosis and pathological diagnosis as well as the development of targeted therapies in OC.

Results

Identification of DEGs from GEO datasets of OC

In the present study, a multistep analysis was carried out to identify candidate genes modulating a certain biological process. First, we selected four GEO datasets of mRNA expression profiling including ovarian cancer and non-tumor ovarian tissue samples. Because of the insufficiency of paracancer tissue in OC, the unpaired non-tumor ovarian tissue was used to replace the paired paracancer tissue. After removing the unqualified samples, 155 tumors and 57 non-tumor samples were included in the subsequent analyses. Second, we aimed to screen DEGs in each GEO dataset with the criteria of log2 is shown in **Figure 1A-1D**. Consequently, 190 consistent genes, including 183 upregulated, and 7 downregulated genes were obtained from the four GEO datasets (**Figure 1E-1F**).

Functional annotation and pathway enrichment analysis of the consistent DEGs

GO and KEGG analysis of the 190 consistent genes was conducted by DAVID. The ten BP categories with the smallest adjusted *p*-value were shown in **Figure 1G**. Five proliferation-associated BP categories were selected and the genes enriched to the categories were shown in the circle plot (**Figure 1H**). Thus, forty proliferation-associated genes were screened. We obtained 17 genes simultaneously enriched to two or more categories of the five proliferation-related ones (SAC3D1, NUF2, FAM83D, TPX2, KIF11, ZWINT, CDCA3, NDC80, PTTG1, BUB1B, KIF15, KI, F18B, SPAG5, CENPF, CDC20, CDK1, and KIF2C), which strongly indicated they were the hub genes and key nodes in the biological process of proliferation. The results of pathway enrichment analysis were shown in **Figure 1I**.

Identification of survival-related genes

Survival analyses of the 17 selected genes were performed by Kalplan Miere Plotter. To obtain genes with more significant prognostic value, we selected overall survival-associated genes with a cutoff of p 0.01. The overall survival curves of the six genes (BUB1B, CDK1, CENPF, FAM83D, KIF15, and TPX2) with significant prognostic value were shown in **Figure 2A-2F**.

To further explore the early-stage prognostic value of these survival-related genes, we conducted OS analysis on the six prognostic genes only in patients of stage I and II. The results showed that higher expression of KIF15 and BUB1B could predict shorter overall survival time than those with lower expression in the early stage of OC (p 0.05) (**Figure 2G, 2I**). Although the sample size of stage I and II patients are quite small, it still provided pieces of evidence that KIF15 and BUB1B appeared to have a differential expression among patients in early stages, suggesting the potential effect of the two genes on prognosis right from the early stages. Thus, the differential expression among stages of the two genes was analyzed by GEPIA (**Figure 2H, 2J**). To resolve the lack of samples of Stage I, we use Stage II to represent the early stage in the analysis. The results certificated that KIF15 and BUB1B began to be overexpressed in early stages, at which the expression of both genes was even higher than that of later stages (stage III and IV). The F value revealed that the KIF15 (F value=5.03) had a greater expressional difference among stages than that of BUB1B (F value=4.7). Significantly higher expression in early stages could provide possibilities for the genes to help to apply early diagnosis and to be a target of early-stage therapeutic intervention. Therefore, KIF15 was selected to be functionally validated because of the more significant expressional difference (greater F value and the smaller *p*-value) among early and late stages.

KIF15 expression level studied in multiple tissues by bioinformatic methods

The KIF15 expression data in multiple normal tissues of females were obtained from the GTEx datasets and visualized (**Figure 3A**). In females, KIF15 has a low expression in major kinds of normal tissues except the bone marrow. To validate the overexpression of KIF15 in OC tissue, the KIF15 expression level of normal ovary samples from GTEx and OC samples from TCGA was compared. The KIF15 expression of OC samples was significantly higher than the normal ovarian samples (**Figure 3B**), consistent with the

results of an analysis of the selected GEO datasets. To further verify the KIF15 overexpression in OC and explore the expression level in other female-specific malignancies, GEPIA online tools were used to conduct the analysis. We also found that except for the previously certified ovarian cancer, KIF15 also significantly overexpressed in Breast invasive carcinoma (BRCA), Cervical squamous cell carcinoma, and endocervical adenocarcinoma (CESC), Uterine Corpus Endometrial Carcinoma (UCEC) and Uterine Carcinosarcoma (UCS) (**Figure 3C**). To preliminarily confirm the feasibility of functional experiments on cell lines, the RNA-seq data of ovarian cell lines from CCLE were downloaded. It showed that KIF15 mRNA was overexpressed in 36/47 ovarian cancer cell lines in CCLE (**Figure 3D**), supporting the feasibility of functional verification on the cellular level.

KIF15 overexpression validated by experimental methods

On TMA of OC, we also validated the overexpression of KIF15 protein on the level of tissue. The samples contained in the online databases such as TCGA are mostly from patients of white. Therefore, we selected a TMA, in which the samples were all from Asians, to apply in the study to figure out whether the KIF15 expression has a racial difference. In the results of TMA analysis, the KIF15 expression of OC samples was significantly higher than that of the unpaired non-tumor ones (p=0.002, **Figure 4A, 4B**). The results also suggested that the overexpression of KIF15 in OC tissues might not have obvious racial differences. We also found that 49/64 OC samples (76.6%) of stage I-II included in the TMA have high expression levels (score 8-12). This was evidence that the upregulation of KIF15 mRNA might originally occur in the early stages of OC and KIF15 was potentially to be a biomarker of early prognosis in OC.

Furthermore, we had validated that ten kinds of cancer cell lines including ovarian cancer (SKOV3, OVCAR3, A2780, and HO8910), cervical cancer (Hela, Siha, and C33a), lung adenocarcinoma (A549), pancreatic cancer (PANC-1), and glioblastoma (U87), all had high expression level of KIF15 mRNA (**Figure 4C**).

Knockdown of KIF15 inhibited proliferation of OC cells *in vitro*

To illuminate the effect of KIF15 knockdown on cell lines with low and high KIF15 original expression level, SKOV3 and HO8910, with relative high, and low KIF15 expression among four common OC cell lines was selected to be functionally studied subsequently. The validity of shRNA lentivirus was verified by both RT-PCR and Western Blot methods (**Figure 5A, 5B**). According to the results of functional annotation, we first assessed the role of KIF15 in OC cell proliferation. Celligo proliferation assay showed that KIF15 knockdown markedly inhibited the proliferation of both SKOV3 and HO8910 cells (**Figure 5C, 5D**) and the results were supported by CCK8 assay (**Figure 5E-5H**). The results suggested that KIF15 acted as a proliferation-promoting oncogene in OC.

Knockdown of KIF15 promoted apoptosis of OC cells *in vitro*

To evaluate whether KIF15 has the potential to be a therapeutic target of OC, we examined the effect of KIF15 knockdown on cell apoptosis by flow cytometry analysis and Caspase 3/7 assay. The most

significant findings were that the knockdown of KIF15 in SKOV3 cells significantly increased the percentage of early apoptotic cells and late apoptotic cells (**Figure 6A-6D**). Similar results were also obtained in the HO8910 cell line. The Caspase 3/7 activity in the SKOV3 and HO8910 samples was increased by KIF15 knockdown, indicating the cell apoptosis was activated (**Figure 6E, 6F**). It revealed that targeting KIF15 might be an effective therapeutic strategy of OC.

Knockdown of KIF15 inhibits tumor formation of OC *in vivo*

To investigate the biological functions of KIF15 *in vivo*, we selected the relatively high-KIF15 expressed SKOV3 cells to perform experiments *in vivo*. The cells of KIF15-KD and NC group were subcutaneously implanted in the corresponding group of Balb/c nude mice. The volume and weight of each tumor were quantified. Under the imager, the green fluorescence of only one mouse with a tumor was observed in the group of ten mice injected with KIF15-KD cells while it was observed in all mice of NC group, indicating that KIF15 knockdown significantly halted tumor formation *in vivo* (**Figure 7A, 7B**). The knockdown of KIF15 resulted in a significant decrease in the volume and weight of tumors as well as the tumor formation ratio (**Figure 7C-7E**). The IHC analysis of xenograft tumor tissues was also visible evidence that knockdown of KIF15 significantly impeded the tumor formation *in vivo* (**Figure 7F**).

KIF15 knockdown promotes OC cell apoptosis via crosstalk among multi-pathways

To further elucidate the mechanisms underlying the apoptosis promotion of KIF15 knock-down, KIF15-KD, and NC cell samples were analyzed by mRNA microarray and phospho-antibody arrays. The same samples were used to extract mRNA and proteins to avoid the batch effect. We obtain 134 upregulated and 309 downregulated DEGs from the mRNA expression profiling after KIF15 knockdown (**Figure 8A**). In the pathway networks constructed by ClueGO, we found that many key DEGs were enriched to the intrinsic apoptosis pathway, TNF signaling pathway, and NF-kappa B (NF-kB) signaling pathway (**Figure 8B**). Consistently, the results of GSEA analysis showed that apoptosis and TNFα signaling via NFkb was the Hallmarks of the DEGs (**Figure 8C**).

To further understand the activation of apoptosis-related pathways, including both the pro-apoptotic and anti-apoptotic pathways after KIF15 knockdown in ovarian cancer cells, we conducted a pathway analysis on the phospho-array results. The phosphorylated proteins on the three apoptosis-related pathways were extracted to build a core network of key phosphorylated proteins (**Figure 8D, 8G**). It was showed that the three pathways have two intersected nodes on mRNA level (Mitogen-Activated Protein Kinase Kinase Kinase 14 [MAP3K14] and Tumor Necrosis Factor [TNF]) and four on protein level (Nuclear Factor Kappa B Subunit 1 [NFkB-p105/p50, Phospho-Ser337], Inhibitor Of Nuclear Factor Kappa B Kinase Subunit Beta [IKK-beta, Phospho-Tyr199], NF-Kappa-B Transcription Factor P65 [NFkB-p65, Phospho-Ser529] and Inhibitor Of Nuclear Factor Kappa B Kinase Regulatory Subunit Gamma [IKK-gamma, Phospho-Ser31]) (**Figure 8E, 8F, 8H**). The networks revealed that the significantly phosphorylated proteins AKT Serine/Threonine Kinase 2 (AKT2), Mitogen-Activated Protein Kinase 1 (MAPK1), BCL2 Apoptosis Regulator (BCL-2), BCL2 Associated X Apoptosis Regulator (BAX), BCL2 Associated Agonist Of Cell Death (BAD), and BH3 Interacting Domain Death Agonist (BID) were key proteins among the three pathways

(**Figure 8G**). The protein expression change and phosphorylation ratio of the key proteins in **Figure 8G** and **8H** were shown in **Table 1**. The phosphorylation ratio greater than 1.12 was considered significant phosphorylation [10]. The results revealed that all the key nodes had a significantly upregulated phosphorylation level, confirming that crosstalk existed among the three apoptosis-related pathways after KIF15 knockdown.

Discussion

The mortality of OC ranks as the first among gynecologic malignant tumors. Because of highly asymptomatic nature and lacking reliable biomarkers, advanced-stage diagnosis and the delayed treatment become the main cause of the high mortality of OC. Investigation of novel and reliable biomarkers with the early prognostic value could facilitate the diagnosis and treatment in the early stages of OC. Uncontrolled proliferation is a crucial character of malignancies and also an important part of cancer development and progression. And inhibiting the sustaining proliferation in cancer could be an effective strategy of target therapies [8]. Here, we used bioinformatics methods to screen the key genes modulating cell proliferation and having a significant impact on the survival time of patients and performed further experimental research.

In the study, a total of 180 overlapped DEGs were obtained based on four datasets of gene expression profiling from GEO. By performing GO analysis, we found that in the top 10 GO categories with the lowest *p*-value, five were correlated to the process of cell mitosis and proliferation. From the five GO categories, we obtained 40 proliferation-related genes, in which 17 genes participated in two or more proliferation-related biological processes. It strongly supported that the 17 genes were the important nodes on the crossroads of the regulatory network modulating the cell function of proliferation. The survival analysis revealed that 6 in the 17 proliferation-related genes had significant prognostic value, including BUB1B, CDK1, CENPF, FAM83D, KIF15, and TPX2. Studies had reported that upregulation of BUB1B, KIF15 [11], CDK1 [12], CENPF [13], FAM83D [14], and *TPX2* [15] all predicted poor prognosis of OC. However, whether these survival-associated genes have early prognostic value in patients of stage I-II has not been reported.

To explore the early prognostic value of these genes, we conducted overall survival analysis on patients of stage I and II and found that the upregulation of BUB1B and KIF15 in early stages could predict poor prognosis of OC patients. It also indicated that these two genes began to be overexpressed and played crucial roles to impact the prognosis of patients in the early stages. Therefore, BUB1B and KIF15 might have the potential to be prognostic indicators, pathological diagnostic biomarkers, and therapeutic targets in early stages in OC. By using GEPIA online tool, we discovered that a greater expressional difference of KIF15 existed between earlier stages (stage II) and later stages (stage III-IV) than BUB1B. The biomarkers with significantly higher expression in early stages might provide a possibility for early diagnosis and targeted therapies in the early stages. Thus, *KIF15* was selected as the candidate gene to be experimentally studied.

KIF15 is a member of kinesin superfamily and a microtubule-associated protein that participated in the mitotic process. Although the structure and molecular functions of KIF15 have been studied for approximately 10 years, the role of KIF15 in the tumorigenesis and progression of OC has not yet been illuminated. A previous study had reported that KIF15 promoted the proliferation of cancer cells in pancreatic cancer [16], bladder cancer [17], breast cancer [18], and osteosarcoma [19]. It indicated that KIF15 was a proliferation-related biomarker in multiple malignancies, which we had verified on ovarian cancer in this study.

The proliferation of cancer cells is an important target of anti-tumor therapeutic strategies. In our study, we found that targeting KIF15 promoted apoptosis of OC cancer cells, highlighting the potential of KIF15 as a therapeutic target to slow down the tumor growth and further delay the progression of OC. Otherwise, we also found that KIF15 overexpressed in five kinds of female-specific cancer but had low expression levels in the corresponding normal tissues. It suggested KIF15 had the potential to be a consistent therapeutic target of female malignancies and simultaneously avoid the off-target effect.

Recent studies had reported that KIF15 was a hub gene associated with cancer stem cell proliferation in lung squamous cell carcinoma [20] by the bioinformatic method of Weighted Gene Co-Expression Network Analysis (WGCNA). Otherwise, KIF15 was also experimentally proved to promote cancer stem cell phenotype and malignancy in hepatocellular carcinoma [21]. These results indicated that KIF15 was not only a target of anti-proliferation therapies of cancers but also a potential target of anti-CSC therapies. However, whether KIF15 plays a CSC-related role in OC and whether the early prognosis value of KIF15 is associated with the stemness maintenance of stem cells from the tumor initial, are still unclear and waiting for further research.

In the present study, the crosstalk of three apoptosis-associated pathways after KIF15 knockdown was discovered by gene expression profiling, and the activation of the was proved by phosphor-antibody arrays. Interestingly, we found that both pro-apoptotic and anti-apoptotic pathways were activated and crosstalked with each other. The intrinsic apoptotic pathway is a vital pro-apoptotic pathway in the apoptotic process of ovarian cancer [22]. However, researchers have reported that NFkb activation could suppress the TNFα-induced apoptosis of cells [23]. By analyzing the result of phosphor-antibody arrays, we found that the TNF signaling pathway was activated. The expression of *RELA* (NFkb-p65), a subunit of NFkb, was upregulated and the protein was significantly phosphorylated, indicating an obvious activation. Moreover, the hub gene AKT2 in the core network, which was upregulated and phosphorylated, playing an anti-apoptosis role in ovarian cancer [24]. We also found that the anti-apoptotic protein BCL-2 was significantly phosphorylated and BCLXL was mildly phosphorylated and expressional upregulated. Otherwise, the pro-apoptotic proteins BAX, BAD, and BID were all significantly activated. The results illuminated that after KIF15 knockdown, the mechanism of anti-apoptosis and pro-apoptosis coexisted. However, according to our experimental research, it showed a pro-apoptotic effect eventually. A recent study had reported that knockdown of KIF15 promoted cell apoptosis in cancer cells, but whether anti-apoptosis mechanisms existed was unclear [19]. If the anti-apoptosis after KIF15 knockdown is a self-

protection mechanism to resist cell death, it strongly supported that KIF15 is an important regulator of cell survival.

Conclusion

In conclusion, we have identified KIF15 as a proliferation-related biomarker with early prognostic and histopathological diagnostic values in OC. Targeting KIF15 inhibited tumor formation growth through restraining proliferation and promoting apoptosis of ovarian cancer cells. The promoted apoptosis of OC cells was regulated by the network constructed by both pro-apoptotic pathways and anti-apoptotic pathways. Therefore, KIF15 may also act as a potential therapeutic target of OC.

Material And Methods

Ethical statement

All animal experiments are in accordance with the "Regulations on the Administration of Laboratory Animals" (The National Science and Technology Commission of the People's Republic of China, March 1, 2017, revised edition) and the National Institutes of Health Laboratory Animal Care and Use Guidelines (ISBN: 13:978-0- 309-15400-0, revised in 2011) to ensure the animal welfare of experimental animals. This study was approved by the Human Research Ethics Committees of Southwest Hospital, Army Medical University (AMU).

OC datasets selection from the GEO database

We selected and downloaded the raw data of four OC datasets from the GEO database. GSE40595 [25] contained 63 high grade serous ovarian cancer samples and 14 normal ovarian samples. GSE18520 [26] contained 53 advanced stages, high-grade primary tumor samples, and 10 normal ovarian samples. GSE38666 [27] contained 25 serous ovarian cancer samples and 20 para-cancer samples. GSE36668 [28] contained 4 serous ovarian borderline tumor samples, 4 well-differentiated serous ovarian carcinomas, and 4 normal ovarian samples. The four datasets were all based on the platform GPL570 (Affymetrix Human Genome U133 Plus 2.0 Array) to reduce the variability from the different experimental setup. Quality analysis was performed on raw data of the selected GEO datasets respectively by using the affyPLM package [29] in R software. Three tumor samples in GSE40595, one tumor sample in GSE18520, and one tumor sample in GSE38666 datasets were removed from the data processing because of the variance of sample quality. Thus, there were 155 tumor samples and 57 non-tumor samples included in our subsequent analysis in total.

Identificaction of proliferation-associated genes from the DEGs

To screen the DEGs in each GEO dataset, the limma package [30] was used with cutoff criteria of |log2 Fold Change (FC)|≥1.5 and adjusted *p*-value≤0.05. The heatmaps were drawn by the tools in the Omicshare platform (https://www.omicshare.com/). For visualization, an online Venn diagram tool

(http://bioinformatics.psb.ugent.be/webtools/Venn/) was used to show the overlapped part of DEGs in the four GEO datasets. The GO and Kyoto Encyclopedia of Genes and Genomes (KEGG) analysis was conducted by DAVID (Resource 6.8) [31]. The top 10 GO categories with the smallest *p*-value and the genes in five proliferation-associated categories ("cell division", "mitotic nuclear division", "cell proliferation", "mitotic sister chromatid segregation", "chromo-some segregation") were visualized by GOplot package in R [32]. The results of pathway enrichment analysis were visualized by using Omicshare tools.

Identification of candidate genes with early prognostic value

The overall survival analysis of the proliferation-associated genes was conducted by the Kal-plan-miere Plotter in all OC patients in the database. To obtain genes with more significant prognostic value, $p<0.01$ was set as the screening criteria. Survival analysis was also performed on the previously obtained prognostic genes only in Stage I-II patients with a cutoff of p 0.05. The different expression among stages of the selected genes with early-stage prognostic value was analyzed in the Gene Expression Profiling Interactive Analysis (GEPIA) database [33]. KIF15 was selected to be bioinformatically analyzed and functionally verified in a subsequent study.

Bioinformatical verification on the expression level of KIF15 in normal and OC tissues

The RNA-seq data of the OC samples in TCGA and normal ovarian samples in GTEx were downloaded from the UCSC Xena project (https://xena.ucsc.edu/). The OC samples (N=379 for cystic, mucinous, and serous neoplasms) was limited to RNA-seq data of FPKM with HTseq and the GTEx samples (N=88 for normal ovarian tissue) was limited to RNAseq data of FPKM. The downloaded RNA-Seq data of both datasets have been recomputed to minimize differences from distinct sources based on a standard pipeline. The corresponding clinical information of the OC dataset was downloaded from the TCGA database (https://portal.gdc.cancer.gov/). The data of KIF15 expression in multiple normal tissue samples of females was extracted and visualized by the ggpubr package in R. The differential expression of KIF15 was visualized by the beeswarm package in R. The analysis of KIF15 differential expression in five kinds of female-specific malignancies was conducted by the GEPIA online tool. The RNA-seq data of KIF15 expression in ovarian cancer cell lines were downloaded from the Cancer Cell Line Encyclopedia (CCLE,https://portals.broadinstitute.org/ccle) [34].

Immunohistochemistry on OC Tissue Microarray

The TMA (Alenabio, Xi'an, China) used in the study contained a total of 100 samples, including 80 ovarian cancer tissue samples of different histological types, 10 lymph node metastasis samples, and 10 non-tumor ovarian samples. The anti-KIF15 rabbit polyclonal antibodies (Sigma-Aldrich Cat# HPA035517) was used to conduct the immunohistochemical staining by a dilution rate of 1:100. The positive staining was quantified and classified into 5 levels: negative staining for 0 score; 1%-25% positive staining cells for 1 score; 26%-50% positive for 2 scores; 51%-75% positive for 3 scores and 76%-100% positive for 4 scores. Staining intensity was scored as negative (0), weak (1), moderate (2),

and robust (3). All the pathologic sections were independently reviewed by two pathologists and the expression levels were graded by the product of positive staining percentage score and staining intensity score.

Cell Culture

The cell lines used in the study, including ovarian cancer cell lines SKOV3, OVCAR-3, A2780, and HO8910, cervical cancer cell lines Hela, Siha and C33A, lung adenocarcinoma cell line A549, pancreatic cancer cell line PANC-1 and glioblastoma cell line U87, were all purchased from the cell bank of Chinese Academy of Science (Shanghai, China). The cell lines were cultured according to the instructions online (http://www.cellbank.org.cn/).

Lentivirus transfection

Human KIF15 knocking down (KD) lentiviruses and negative control (NC) lentiviruses were constructed by Genechem (Shanghai, China). SKOV3 and HO8910 cells were seeded in 6-well plates the day before transduction to ensure the cells would grow to 30% to 40% confluence the next day, and then infected with lentivirus for 24 h at a Multiplicity Of Infection (MOI) of 20 and 10 respectively in the presence of polybrene (5 mg/mL, Genechem).

qRT-PCR analysis

The qRT-PCR was performed as previously reported [35]. The $2^{-\Delta\Delta ct}$ method was used to determine the expression of the KIF15 gene. All experiments were carried out in triplicate. The primers were purchased from Sangon Biotech (Shanghai, China).

KIF15:

Forward 5 '- CTCTCACAGTTGAATGTCCTTG - 3'

Reverse 5 '- CTCCTTGTCAGCAGAATGAAG - 3'

GAPDH:

Forward 5 '- TGACTTCAACAGCGACACCCA - 3 '

Reverse 5 '- CACCCTGTTGCTGTAGCCAAA - 3 '

Western Blot analysis

Western Blot was performed as previously described [35]. GAPDH was used as a loading control. The KIF15 rabbit polyclonal antibody (1:100) and GAPDH monoclonal antibody (1:1000, Santa Cruz Biotechnology Cat# sc-32233) was used.

Cell growth analysis by Celigo method

SKOV3 and HO8910 cells were transfected with KIF15-KD or NC lentivirus. The transfected cells were collected and then seeded into 48-well plates 2000 cells per well respectively. The number of cells with green fluorescence in each well was measured by a Cellomics ArrayScan System (Nexcelom, USA) once a day. The variable data of the green fluorescence signal were obtained for statistical analysis to construct 5-day cell proliferation curves. The green-fluorescence cells were also scanned to be counted by an image analysis software. The count of green-fluorescence cells at each time point was compared with that of day 1 to calculate the cell proliferation ratio for each time point and each experimental group. The fold change of cell proliferation was obtained to construct cell growth curves.

The cell proliferation ratio was computed as follows: fold change (NC vs experimental group)= proliferation ratio on day 5 for the NC group/proliferation ratio on day 5 for the experimental group. A fold change of proliferation ratio equal to or greater than 2 indicated that cell proliferation had been significantly slowed down.

Cell Counting Kit-8 (CCK8) assay

SKOV3 and HO8910 cells were plated into 96-well plates at some 2000 cells per well and transfected with the KIF15-KD or NC lentivirus. Cell proliferation was measured by using CCK8 Reagent (DOJINDO, JAPAN) respectively on days 1, 2, 3, 4, and 5 after transfection. The assays were performed in triplicate.

FACS assay by flow cytometry

Cells were seeded into 6-well plates and cultured in serum-free medium at 37°C for 24 h. Cells were transfected with the KIF15-KD or NC lentiviruses. Then the cells were harvested and analyzed by an AnnexinV-APC apoptosis kit (eBioscience, USA). Cell apoptosis was determined using the Guava InCyte software (Millipore, USA). All experiments were conducted in triplicate.

Caspase3/7 activity assay

To assess the activity of caspases 3 and 7, the Caspase-Glo 3/7 Assay (Promega, Germany) was conducted following the manufacturer's instructions. The Caspase-Glo 3/7 Assay is based on the cleavage of the DEVD sequence of a luminogenic substrate by the caspases 3 and 7 and results in a luminescent signal. The fluorescence signal was measured at an excitation wavelength of 485 nm and an emission wavelength of 527 nm.

Subcutaneous transplantation of human OC cells in Balb/c nude mice

Female Balb/c nude mice of four weeks old were used in this experiment. A total of 2×10^7 transfected SKOV3 cells were subcutaneously injected into the right armpit of each mouse. The body weight and tumor diameter of each mouse were measured every week after cell transplantation. All mice were sacrificed on the 41st day after the initiation of cell injection. Before the mice were killed, the fluorescence images of xenograft tumors were photographed under a whole-body fluorescent imaging system (Lumina LT, Perkin Elmer, USA). Tumors were observed by both macroscopical and microscopical methods.

mRNA expression profiling

The SKOV3 cells of KIF15-KD and NC group were collected for mRNA expression profiling. Total RNA was isolated from cell samples by using an Agilent RNA 6000 Nano Kit (Agilent, USA), and the quality of total RNA was analyzed. Both the KIF15-KD and NC cell samples had three replicates. The mRNA expression profiling was conducted by using GeneChip prime view humans (901838, Affymetrix, USA). RNA labeling and hybridization were performed with a GeneChip Hybridization Wash and Stain Kit (Agilent, USA). The raw data obtained from mRNA expression profiling was quality-analyzed using R software as the aforementioned methods in Paragraph 2.2 before subsequent bioinformatic analysis.

Phospho-antibody arrays

To avoid batch difference, the cell samples applied in mRNA expression profiling were examined in this assay. The cell lysates of KIF15-KD and NC group were obtained and applied to a Cancer Signaling Phospho-Antibody Array ((PCS300, Full Moon Biosystems, USA). The phosphoantibody array detection was carried out in cooperation with Wayne Biotechnology (Shanghai, China) per the manufacturer's protocols. The array contained 157 site-specific and phospho-specific antibodies and 147 non-phospho antibodies, each of which had 6 replicates. The slides were scanned by a GenePix 4000 scanner and the images were analyzed with GenePix Pro 6.0 (Molecular Devices, Sunnyvale, CA). The intensity of the fluorescence signal obtained from each antibody-stained region indicated the expression level of a certain protein. The extent of protein phosphorylation was measured by a ratio computation. The phosphorylation ratio was calculated as follows: phosphorylation ratio=phospho value/non-phosphor value [36]. The total proteome ratios were standardized by β-actin.

Pathway analysis by multiple bioinformatics methods

The DEGs in mRNA expression profiling were obtained by using R packages with a cutoff of |Fold Change|≥1.5 and p□0.05. The pathway analysis was performed with the plug-in ClueGO [37] in Cytoscape software (Version 3.7.1) with a cutoff of p□0.05. GSEA (Version 3.0), a pathway enrichment method was also used to analyze a level of gene sets. GSEA software uses the predefined gene sets from the Molecular Signatures Database (MSigDB v6.2) [38]. A gene set is a group of genes that share similar pathways, functions, chromosomal localization, or other features. In this study, we used all the C collection sets for GSEA analysis (i.e., H, C1-C7 collection in MsigDB). The list of ranked genes based on a score calculated as -log10 of p-value multiplied by the sign of fold change. The minimum and maximum criteria for the selection of gene sets from the collection were 10 and 500 genes, respectively. Pathway enrichment analysis on the results of the phos-pho-antibody arrays was also performed. According to the pathways obtained by using DAVID and GSEA, the phosphorylated proteins on the pathways were selected and the protein-protein interactive (PPI) networks were visualized by Cytoscape. The consistent genes and phosphorylated proteins on the previously obtained pathways both in mRNA expression microarrays and phospho-antibody arrays were visualized by Venn tools in the Omicshare platform.

Statistical analysis

SPSS 20.0 (IBM SPSS, Chicago, IL) software was used for statistical analyses. Values are presented as the mean±SD. Wilcox test was used to determine the significant expression difference of DEGs among ovarian cancer and non-tumor samples in GEO and TCGA datasets. The differences between NC and KD groups in proliferation and apoptosis assays were tested by the Student's t-test. The different expression levels between the ovarian cancer tissue samples and adjacent non-tumor samples in TMA were tested with the Mann-Whitney test. $p<0.05$ was considered statistically significant.

Declarations

Ethics approval and consent to participate

All animal experiments are in accordance with the "Regulations on the Administration of Laboratory Animals" (The National Science and Technology Commission of the People's Republic of China, March 1, 2017, revised edition) and the National Institutes of Health Laboratory Animal Care and Use Guidelines (ISBN: 13:978-0- 309-15400-0, revised in 2011) to ensure the animal welfare of experimental animals. This study was approved by the Human Research Ethics Committees of SouthwestHospital,Army Medical University(AMU).

Consent for publication

Not applicable.

Availability of data and materials

The data used and/or analysed during the current study are available from the corresponding author on reasonable request.

Conflict of interest

The authors declare that they have no competing interests.

Funding

This work was supported by the National Key Technology R&D Program of China (No.2019YFC1005202 and 2019YFC1005204) and the Clinical Innovation Foundation of Southwest Hospital of China (No.SWH2016ZDCX1013).

Authors' contributions

Xinwei Sun, Mengyue Chen, Bin Liao, and Zhiqing Liang performed all the experiments and analyses. Xinwei Sun, Mengyue Chen, and Zhiqing Liang were responsible for the study design, data interpretation and writing. All authors read and approved the final manuscript.

Acknowledgements

Not applicable.

References

1. Torre LA, Trabert B, DeSantis CE, Miller KD, Samimi G, Runowicz CD, Gaudet MM, Jemal A, Siegel RL. Ovarian cancer statistics, 2018. CA Cancer J Clin. 2018;68:284-96.
2. Xi QP, Pu DH, Lu WN. Research on application value of combined detection of serum CA125, HE4 and TK1 in the diagnosis of ovarian cancer. Eur Rev Med Pharmacol Sci. 2017;21:4536-41.
3. Dizon DS. PARP inhibitors for targeted treatment in ovarian cancer. Lancet. 2017;390:1929-30.
4. Edgar R, Domrachev M, Lash AE. Gene Expression Omnibus: NCBI gene expression and hybridization array data repository. Nucleic Acids Res. 2002;30:207-10.
5. Cancer Genome Atlas Research N, Weinstein JN, Collisson EA, Mills GB, Shaw KR, Ozenberger BA, Ellrott K, Shmulevich I, Sander C, Stuart JM. The Cancer Genome Atlas Pan-Cancer analysis project. Nat Genet. 2013;45:1113-20.
6. Zheng MJ, Li X, Hu YX, Dong H, Gou R, Nie X, Liu Q, Ying-Ying H, Liu JJ, Lin B. Identification of molecular marker associated with ovarian cancer prognosis using bioinformatics analysis and experiments. J Cell Physiol. 2019;234:11023-36.
7. Yang X, Zhu S, Li L, Zhang L, Xian S, Wang Y, Cheng Y. Identification of differentially expressed genes and signaling pathways in ovarian cancer by integrated bioinformatics analysis. Onco Targets Ther. 2018;11:1457-74.
8. Feitelson MA, Arzumanyan A, Kulathinal RJ, Blain SW, Holcombe RF, Mahajna J, Marino M, Martinez-Chantar ML, Nawroth R, Sanchez-Garcia I, Sharma D, Saxena NK, Singh N, Vlachostergios PJ, Guo S, Honoki K, Fujii H, Georgakilas AG, Bilsland A, Amedei A, Niccolai E, Amin A, Ashraf SS, Boosani CS, Guha G, Ciriolo MR, Aquilano K, Chen S, Mohammed SI, Azmi AS, Bhakta D, Halicka D, Keith WN, Nowsheen S. Sustained proliferation in cancer: Mechanisms and novel therapeutic targets. Semin Cancer Biol. 2015;35 Suppl:S25-s54.
9. Fekete JT, Ősz Á, Pete I, Nagy GR, Vereczkey I, Győrffy B. Predictive biomarkers of platinum and taxane resistance using the transcriptomic data of 1816 ovarian cancer patients. Gynecol Oncol. 2020;156:654-61.
10. Zhang YM, Dai BL, Zheng L, Zhan YZ, Zhang J, Smith WW, Wang XL, Chen YN, He LC. A novel angiogenesis inhibitor impairs lovo cell survival via targeting against human VEGFR and its signaling pathway of phosphorylation. Cell Death Dis. 2012;3:e406.
11. Feng H, Gu ZY, Li Q, Liu QH, Yang XY, Zhang JJ. Identification of significant genes with poor prognosis in ovarian cancer via bioinformatical analysis. J Ovarian Res. 2019;12:35.
12. Xi Q, Huang M, Wang Y, Zhong J, Liu R, Xu G, Jiang L, Wang J, Fang Z, Yang S. The expression of CDK1 is associated with proliferation and can be a prognostic factor in epithelial ovarian cancer. Tumour Biol. 2015;36:4939-48.

13. Xu Z, Zhou Y, Cao Y, Dinh TL, Wan J, Zhao M. Identification of candidate biomarkers and analysis of prognostic values in ovarian cancer by integrated bioinformatics analysis. Med Oncol. 2016;33:130.
14. Zhang Q, Yu S, Lok SIS, Wong AST, Jiao Y, Lee LTO. FAM83D promotes ovarian cancer progression and its potential application in diagnosis of invasive ovarian cancer. J Cell Mol Med. 2019;23:4569-81.
15. Cáceres-Gorriti KY, Carmona E, Barrès V, Rahimi K, Létourneau IJ, Tonin PN, Provencher D, Mes-Masson AM. RAN nucleo-cytoplasmic transport and mitotic spindle assembly partners XPO7 and TPX2 are new prognostic biomarkers in serous epithelial ovarian cancer. PLoS One. 2014;9:e91000.
16. Wang J, Guo X, Xie C, Jiang J. KIF15 promotes pancreatic cancer proliferation via the MEK-ERK signalling pathway. Br J Cancer. 2017;117:245-55.
17. Zhao H, Bo Q, Wu Z, Liu Q, Li Y, Zhang N, Guo H, Shi B. KIF15 promotes bladder cancer proliferation via the MEK-ERK signaling pathway. Cancer Manag Res. 2019;11:1857-68.
18. Sheng J, Xue X, Jiang K. Knockdown of Kinase Family 15 Inhibits Cancer Cell Proliferation In vitro and its Clinical Relevance in Triple-Negative Breast Cancer. Curr Mol Med. 2019;19:147-55.
19. Wu Z, Zhang H, Sun Z, Wang C, Chen Y, Luo P, Yan W. Knockdown of Kinesin Family 15 Inhibits Osteosarcoma through Suppressing Cell Proliferation and Promoting Cell Apoptosis. Chemotherapy. 2019;64:187-96.
20. Qin S, Long X, Zhao Q, Zhao W. Co-Expression Network Analysis Identified Genes Associated with Cancer Stem Cell Characteristics in Lung Squamous Cell Carcinoma. Cancer Invest. 2020;38:13-22.
21. Li Q, Qiu J, Yang H, Sun G, Hu Y, Zhu D, Deng Z, Wang X, Tang J, Jiang R. Kinesin family member 15 promotes cancer stem cell phenotype and malignancy via reactive oxygen species imbalance in hepatocellular carcinoma. Cancer Lett. 2020;482:112-25.
22. Nordin N, Fadaeinasab M, Mohan S, Mohd Hashim N, Othman R, Karimian H, Iman V, Ramli N, Mohd Ali H, Abdul Majid N. Pulchrin A, a New Natural Coumarin Derivative of Enicosanthellum pulchrum, Induces Apoptosis in Ovarian Cancer Cells via Intrinsic Pathway. PLoS One. 2016;11:e0154023.
23. Van Antwerp DJ, Martin SJ, Kafri T, Green DR, Verma IM. Suppression of TNF-alpha-induced apoptosis by NF-kappaB. Science. 1996;274:787-9.
24. Ding Z, Xu F, Li G, Tang J, Tang Z, Jiang P, Wu H. Knockdown of Akt2 expression by shRNA inhibits proliferation, enhances apoptosis, and increases chemosensitivity to paclitaxel in human colorectal cancer cells. Cell Biochem Biophys. 2015;71:383-8.
25. Yeung TL, Leung CS, Wong KK, Samimi G, Thompson MS, Liu J, Zaid TM, Ghosh S, Birrer MJ, Mok SC. TGF-β modulates ovarian cancer invasion by upregulating CAF-derived versican in the tumor microenvironment. Cancer Res. 2013;73:5016-28.
26. Mok SC, Bonome T, Vathipadiekal V, Bell A, Johnson ME, Wong KK, Park DC, Hao K, Yip DK, Donninger H, Ozbun L, Samimi G, Brady J, Randonovich M, Pise-Masison CA, Barrett JC, Wong WH, Welch WR, Berkowitz RS, Birrer MJ. A gene signature predictive for outcome in advanced ovarian cancer identifies a survival factor: microfibril-associated glycoprotein 2. Cancer Cell. 2009;16:521-32.

27. Lili LN, Matyunina LV, Walker LD, Benigno BB, McDonald JF. Molecular profiling predicts the existence of two functionally distinct classes of ovarian cancer stroma. Biomed Res Int. 2013;2013:846387.
28. Elgaaen BV, Olstad OK, Sandvik L, Odegaard E, Sauer T, Staff AC, Gautvik KM. ZNF385B and VEGFA are strongly differentially expressed in serous ovarian carcinomas and correlate with survival. PLoS One. 2012;7:e46317.
29. Heber S, Sick B. Quality assessment of Affymetrix GeneChip data. OMICS. 2006;10:358-68.
30. Ritchie ME, Phipson B, Wu D, Hu Y, Law CW, Shi W, Smyth GK. limma powers differential expression analyses for RNA-sequencing and microarray studies. Nucleic Acids Res. 2015;43:e47.
31. Huang da W, Sherman BT, Lempicki RA. Bioinformatics enrichment tools: paths toward the comprehensive functional analysis of large gene lists. Nucleic Acids Res. 2009;37:1-13.
32. Walter W, Sánchez-Cabo F, Ricote M. GOplot: an R package for visually combining expression data with functional analysis. Bioinformatics. 2015;31:2912-4.
33. Tang Z, Li C, Kang B, Gao G, Li C, Zhang Z. GEPIA: a web server for cancer and normal gene expression profiling and interactive analyses. Nucleic Acids Res. 2017;45:W98-w102.
34. Pharmacogenomic agreement between two cancer cell line data sets. Nature. 2015;528:84-7.
35. Yu X, He X, Heindl LM, Song X, Fan J, Jia R. KIF15 plays a role in promoting the tumorigenicity of melanoma. Exp Eye Res. 2019;185:107598.
36. Liu D, Zhang XX, Li MC, Cao CH, Wan DY, Xi BX, Tan JH, Wang J, Yang ZY, Feng XX, Ye F, Chen G, Wu P, Xi L, Wang H, Zhou JF, Feng ZH, Ma D, Gao QL. C/EBPβ enhances platinum resistance of ovarian cancer cells by reprogramming H3K79 methylation. Nat Commun. 2018;9:1739.
37. Bindea G, Mlecnik B, Hackl H, Charoentong P, Tosolini M, Kirilovsky A, Fridman WH, Pagès F, Trajanoski Z, Galon J. ClueGO: a Cytoscape plug-in to decipher functionally grouped gene ontology and pathway annotation networks. Bioinformatics. 2009;25:1091-3.
38. Liberzon A, Birger C, Thorvaldsdóttir H, Ghandi M, Mesirov JP, Tamayo P. The Molecular Signatures Database (MSigDB) hallmark gene set collection. Cell Syst. 2015;1:417-25.

Tables

Table 1
The fold change of key proteins in the crosstalk of apoptosis-associated pathways.

Key Proteins	Ratio (KD vs NC)
AKT2	1.15
AKT2 (Phospho-Ser474)	1.30
BAD (Phospho-Ser136)	1.29
BAX	1.02
BAX (Phospho-Thr167)	1.25
BCL-2 (Phospho-Ser70)	1.33
BID	1.05
BID (Phospho-Ser78)	1.29
p44/42 MAP Kinase	1.19
p44/42 MAP Kinase (Phospho-Tyr204)	1.27
IKK α/β	1.15
IKKα/β(Phospho-Ser180/181)	1.20
PLCG1	1.25
PLCG1 (Phospho-Tyr783)	1.21
RelB	1.20
RelB (Phospho-Ser552)	1.24
NFkB-p105/p50	0.98
NFkB-p105/p50 (Phospho-Ser337)	1.15
IKK-β	1.21
IKK-β(Phospho-Tyr199)	1.18
NFkB-p65	1.25
NFkB-p65 (Phospho-Ser529)	1.29
IKK-γ	1.13
IKK-γ (Phospho-Ser31)	1.15

Figures

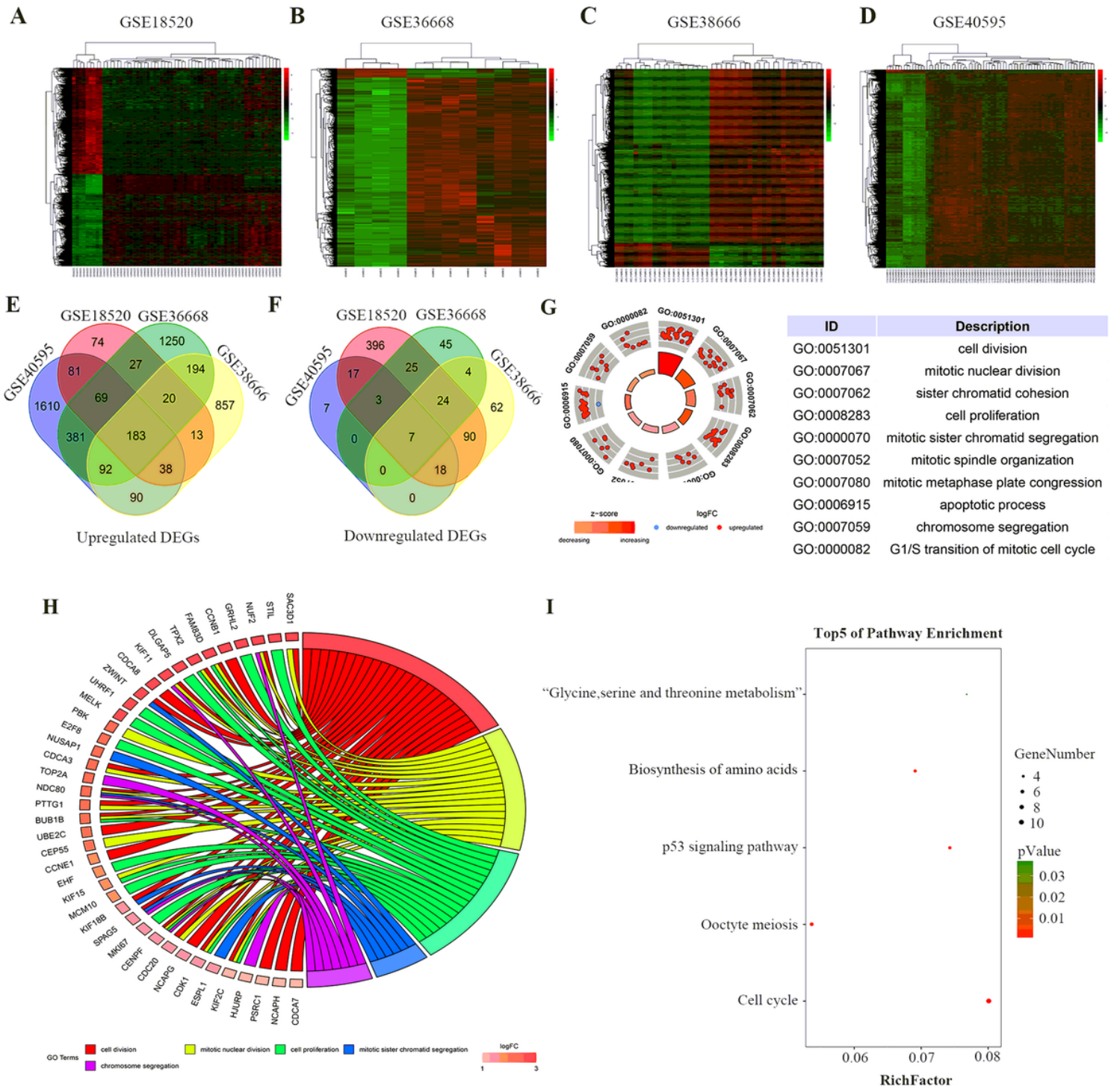

Figure 1

Identification of DEGs from four GEO datasets of OC and the functional and pathway enrichment analysis of consistent DEGs of the datasets. (A-D) The heatmaps of DEGs from four datasets of gene expression profiling. (E, F) The overlapped part of upregulated and downregulated DEGs in four OC datasets. (G) The ten GO categories with the smallest p-value. (H) The genes in five proliferation-associated BP categories. (I) The KEGG pathway analysis of the overlapped part of DEGs from four GEO datasets.

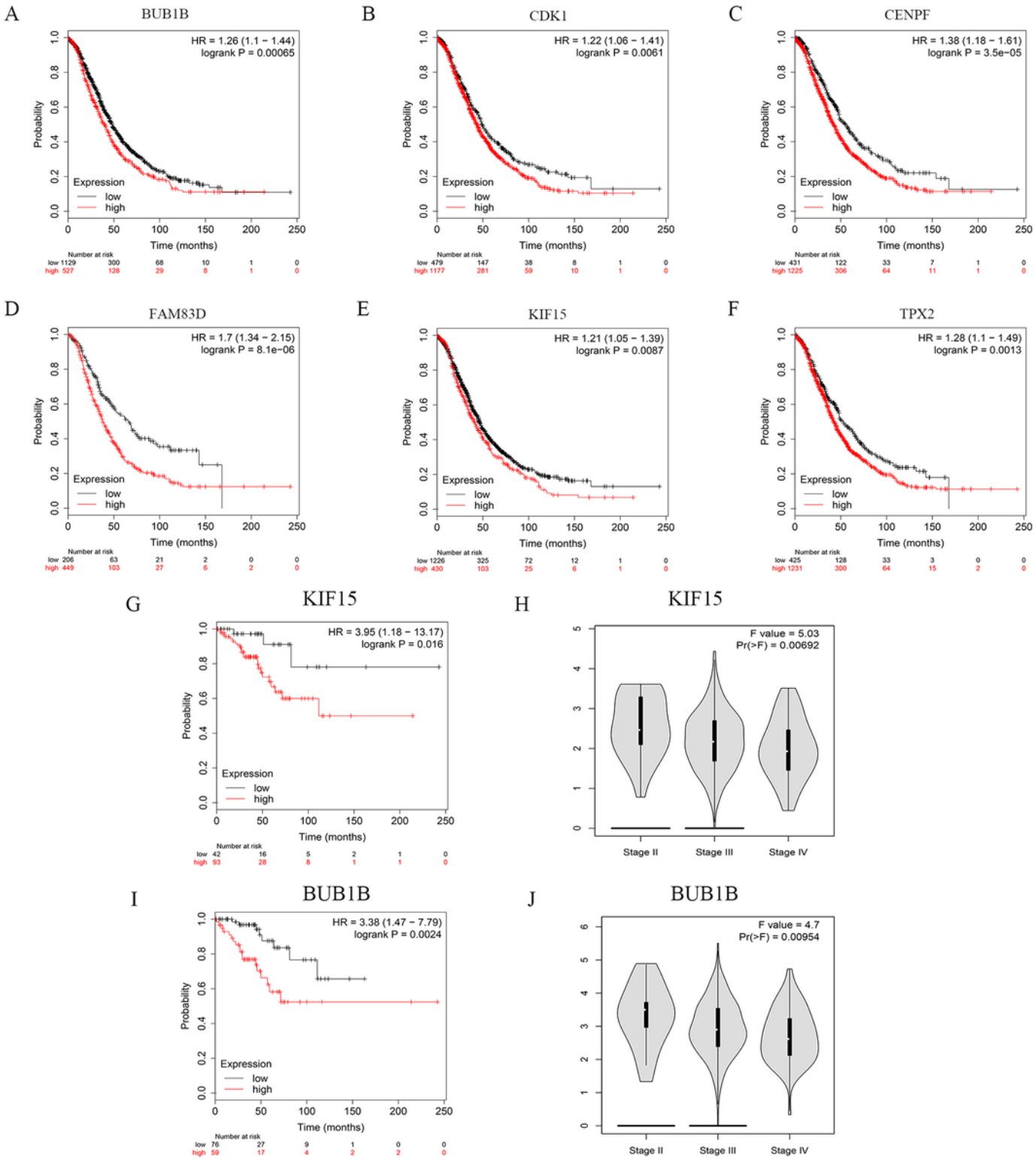

Figure 2

Identification of survival-associated genes. (A-F) Identification of overall survival associated DEGs (p 0.01). (G, I) Identification of overall survival associated DEGs (KIF15 and BUB1B) in patients of stage I and II (p0.05). (H, J) The differential expression of KIF15 and BUB1B among stages (p0.05).

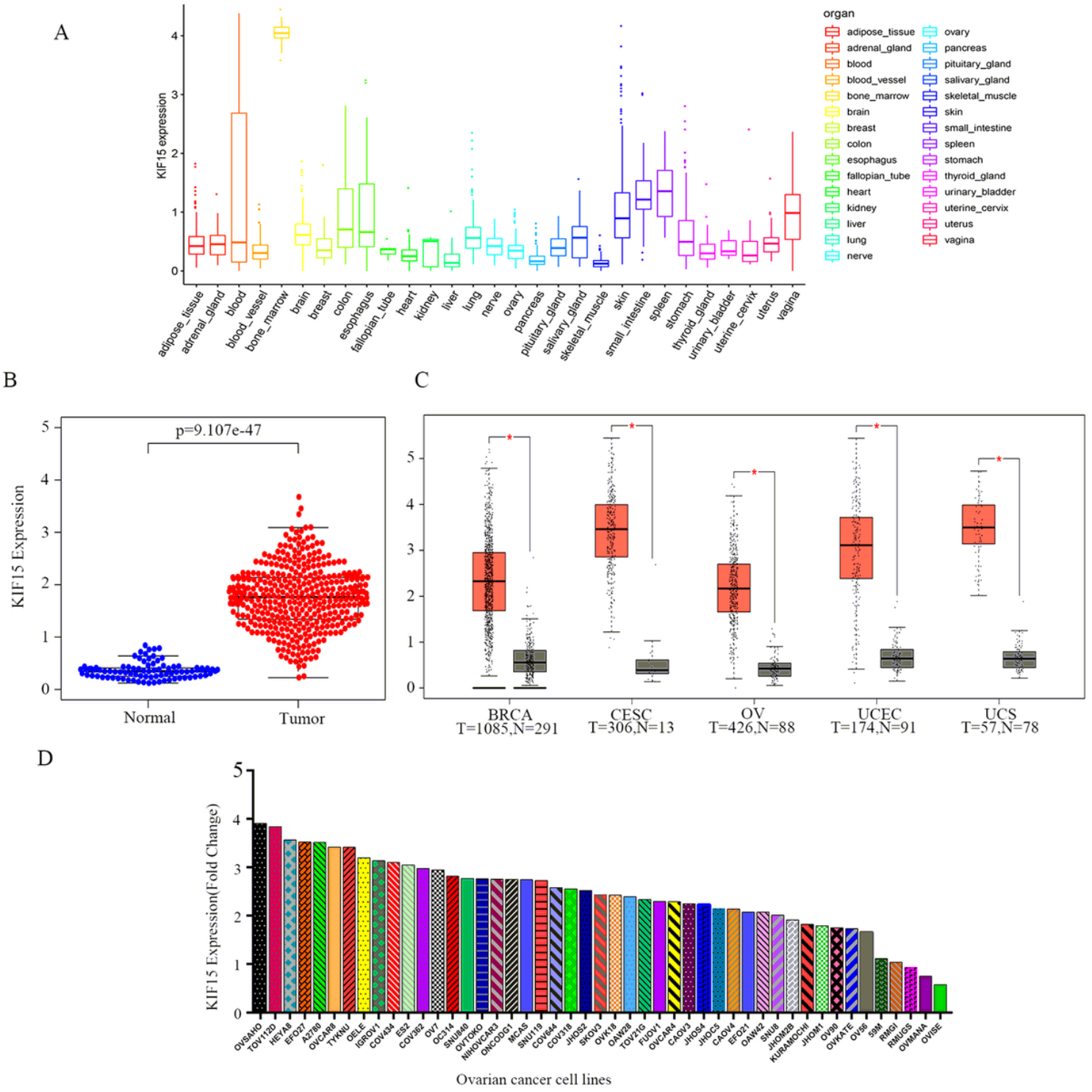

Figure 3

KIF15 expression in tissues and ovarian cancer cell lines by bioinformatic analysis. (A) KIF15 expression level in multiple normal tissues of females. (B) The comparison of KIF15 expression level between normal ovarian tissue and ovarian cancer samples (p□0.05). (C) KIF15 overexpression in five female-specific malignancies (Red boxplots represented ovarian cancer samples, gray boxplots represented normal ovarian tissues. *represented p□0.05). (D) KIF15 expression in ovarian cancer cell lines.

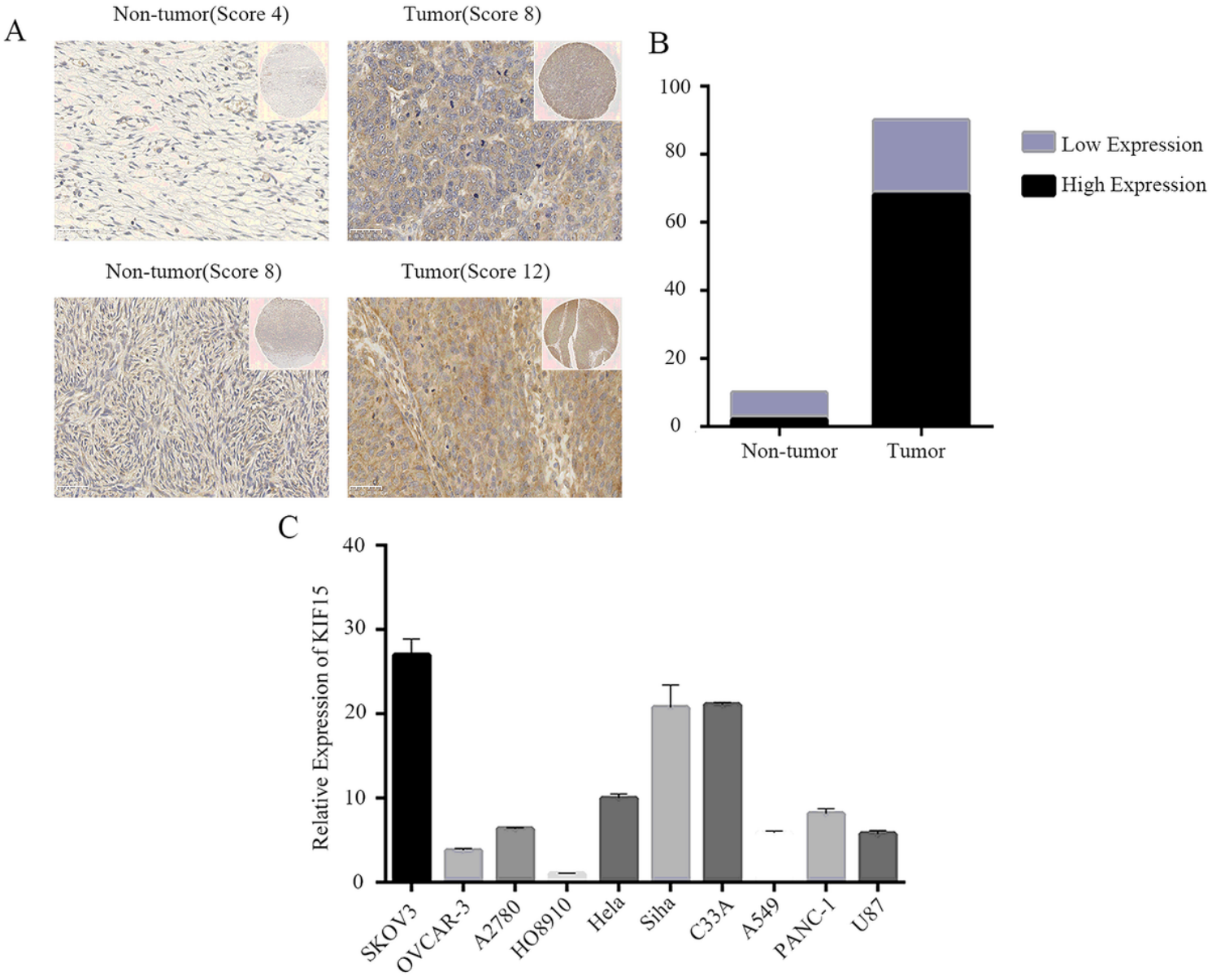

Figure 4

KIF15 overexpression in TMA and multiple cancer cell lines validated by experimental methods. (A) Immunohistochemistry on TMA of OC. (B) The sample size of low and high expression in adjacent and tumor tissues (Score≤8 represented low expression, score 8-12 represented high expression). (C) The expression level of KIF15 in cancer cell lines.

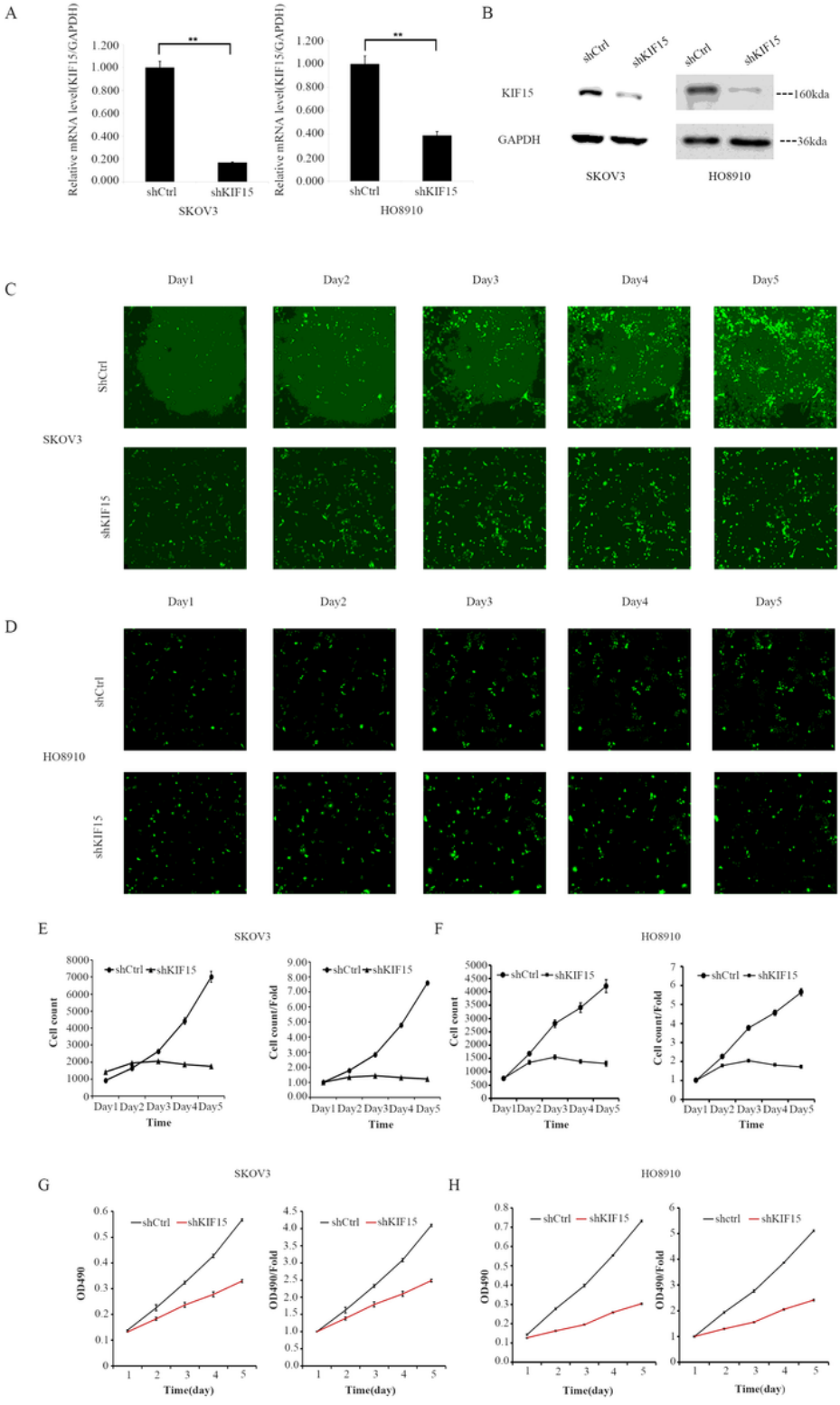

Figure 5

The knockdown of KIF15 inhibits the proliferation of OC cells in vitro. (A, B) The validity of shRNA lentivirus verified by RT-PCR (**represented p□0.01) and western blot. (C, D) KIF15 knockdown inhibited SKOV3 and HO8910 proliferation analyzed by the Celigo method. (E, F) The variation trend of cell count and cell count fold change of SKOV3 and HO8910 cell lines. (G, H) KIF15 knockdown inhibited SKOV3 and HO8910 proliferation analyzed by the CCK8 method.

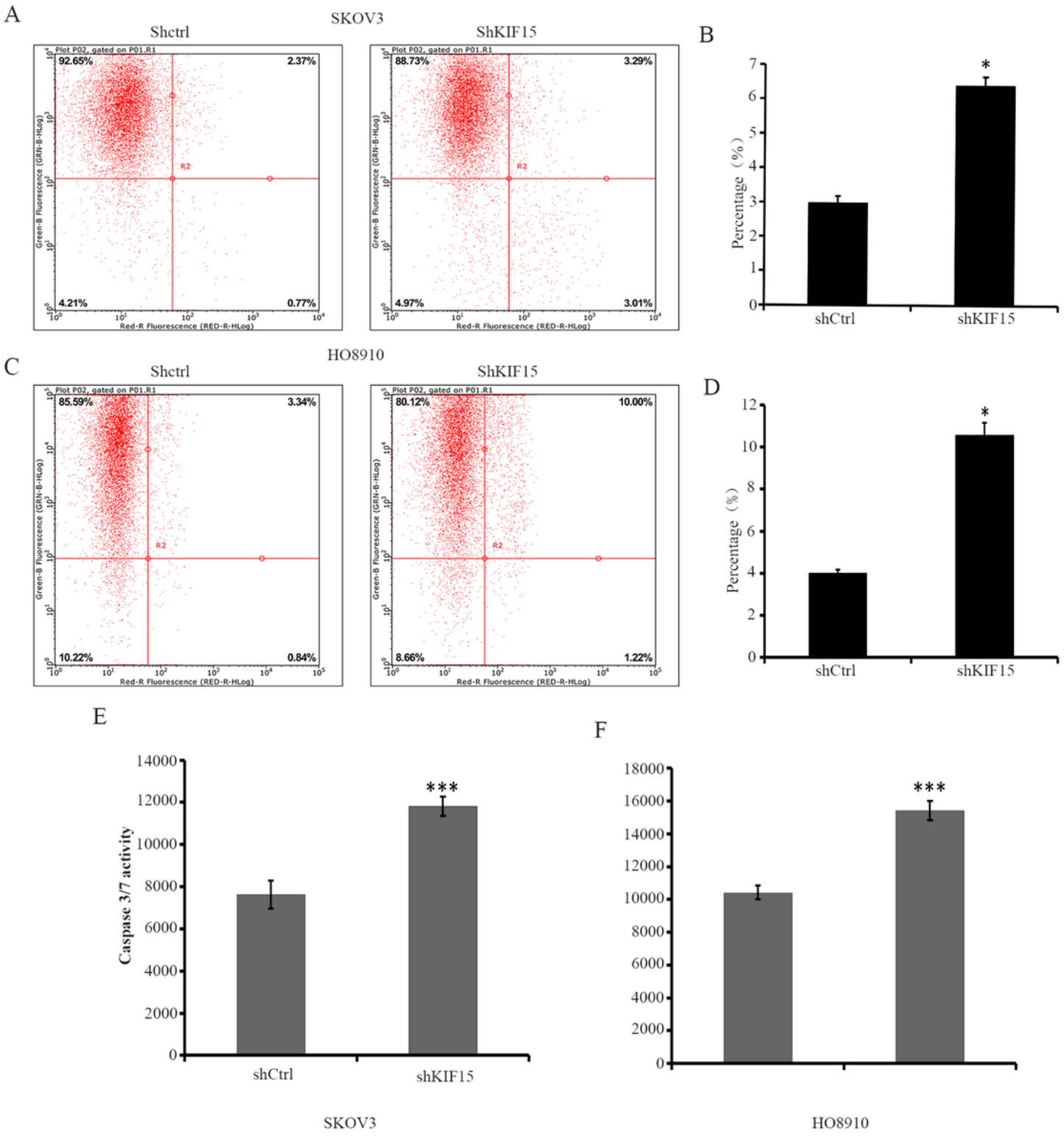

Figure 6

Knockdown of KIF15 promoted apoptosis of OC cells in vitro. (A-D) The cell apoptosis of SKOV3 and HO8910 was analyzed by the flow cytometry method. (E, F) Cell apoptosis was analyzed by Caspase 3/7 assay. (*represented p□0.05, ***represented p□0.001).

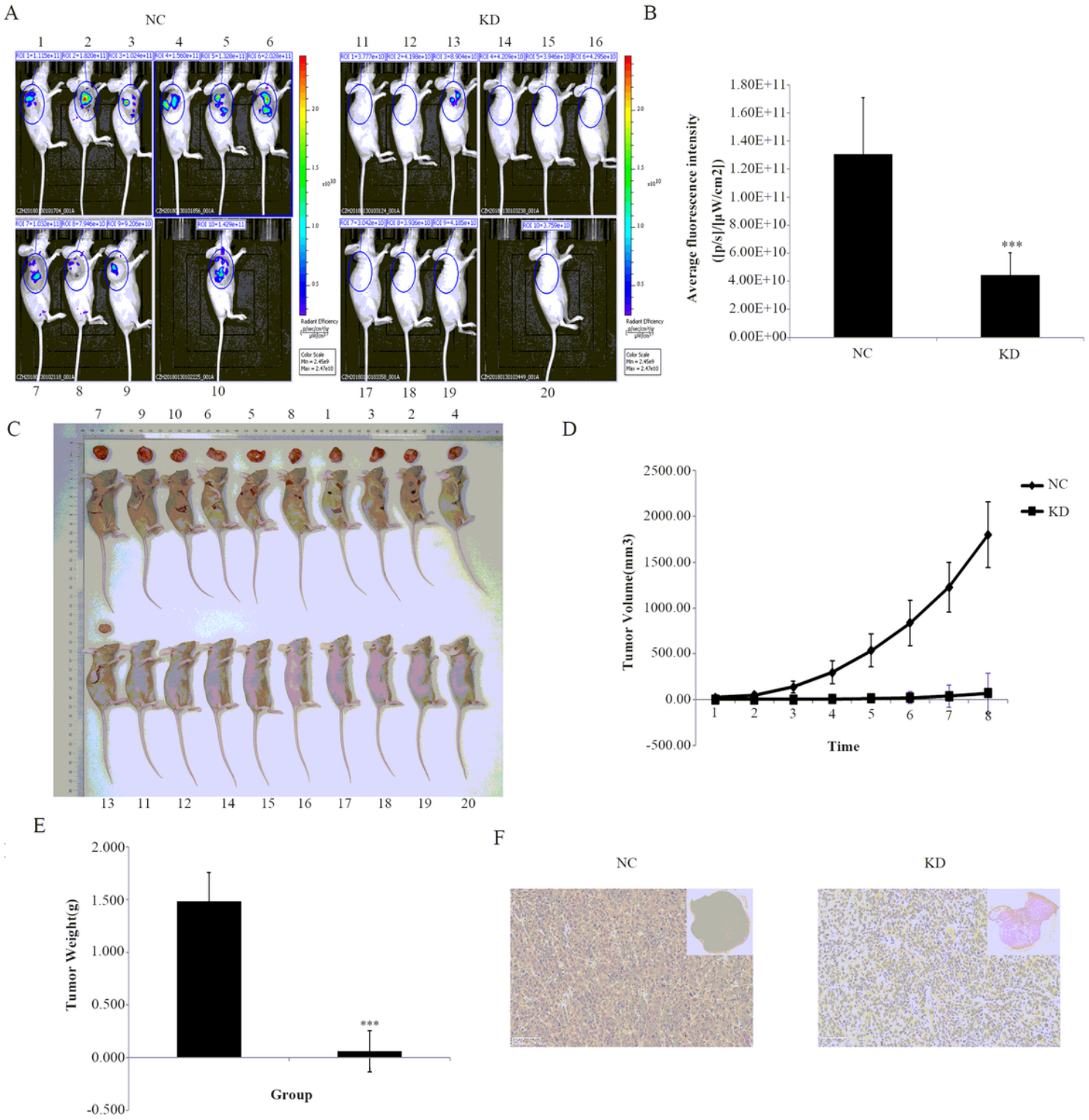

Figure 7

The knockdown of KIF15 inhibited tumor formation of OC in vivo. (A) The green fluorescence signal of xenograft tumor in mice of NC and KD groups. The mice were numbered 1-10 (NC group), and 11-20 (KD group). (B) The average fluorescence intensity of xenograft tumors in mice of NC and KD groups. (C) The xenograft tumors and mice of NC and KD groups. (D) The variation trend of average tumor volume in NC,

and KD groups. (E) The average tumor weight of NC and KD groups. (F) The KIF15 expression in xenograft tumors of NC and KD groups analyzed by IHC methods (***represented p□0.001).

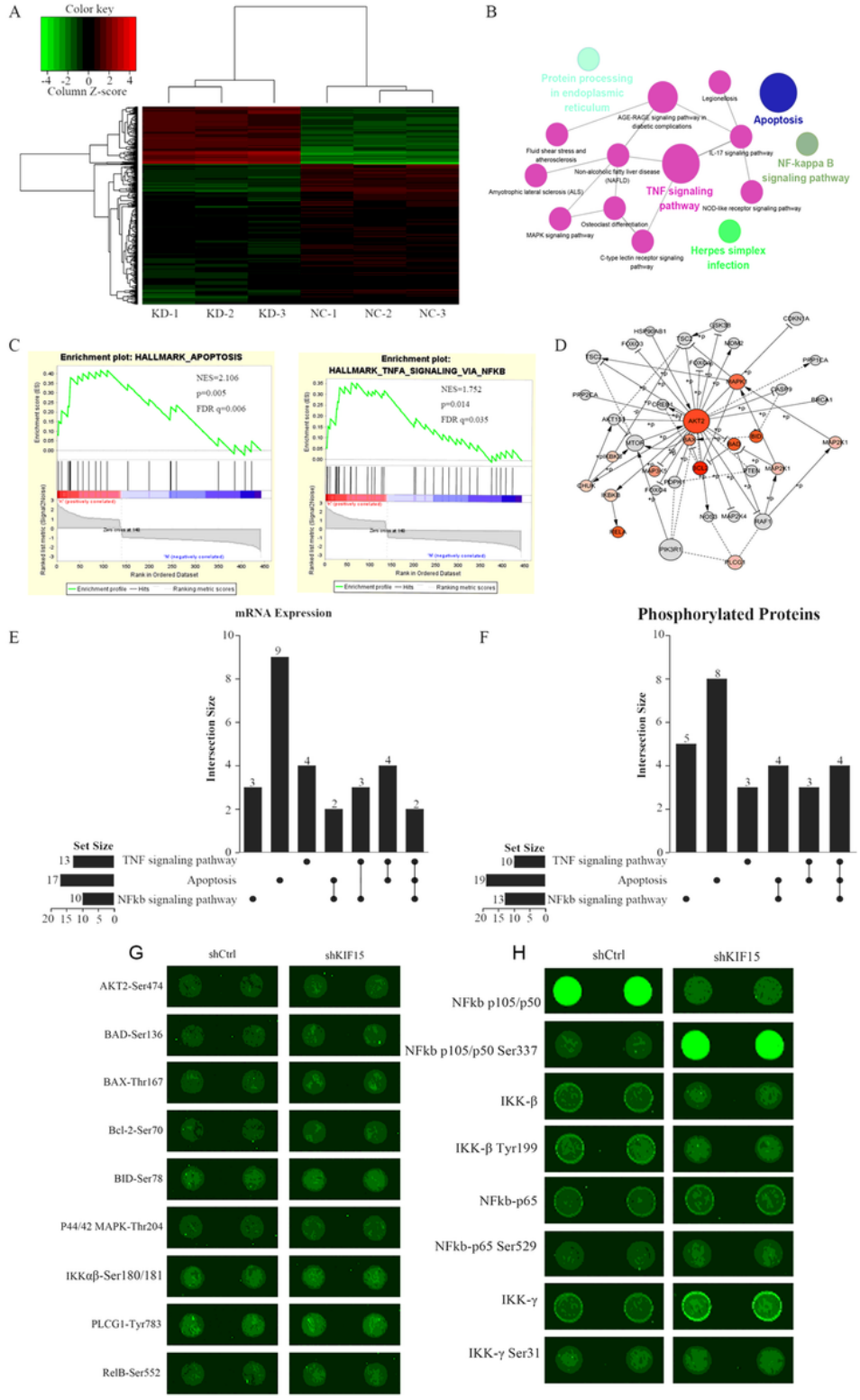

Figure 8

KIF15 knockdown promotes OC cell apoptosis via crosstalk between multi-pathways. (A) The heatmap of DEGs obtained from the gene expression profiling after KIF15 knockdown. (B) The pathway networks were constructed among the DEGs. (C) The hallmarks of the DEGs were analyzed by GSEA. (D) The core

networks of the key phosphorylated proteins among three apoptosis-related pathways. (E, F) The common nodes of three apoptosis-related pathways in mRNA and phosphorylated protein levels. (G) The significantly phosphorylated proteins in the core networks. (H) The protein and phosphorylated protein expression levels of the four intersected nodes in the three apoptosis-related pathways at the protein level.